

**UCLA**

**UCLA Previously Published Works**

**Title**

Intramolecular N–H···F Hydrogen Bonding Interaction in a Series of 4-Anilino-5-Fluoroquinazolines: Experimental and Theoretical Characterization of Electronic and Conformational Effects

**Permalink**

<https://escholarship.org/uc/item/8zt672z9>

**Journal**

Chemistry - A European Journal, 28(2)

**ISSN**

0947-6539

**Authors**

Urner, Lorenz M  
Lee, Ga Young  
Treacy, Joseph W  
et al.

**Publication Date**

2022-01-10

**DOI**

10.1002/chem.202103135

Peer reviewed



Published in final edited form as:

Chemistry. 2022 January 10; 28(2): e202103135. doi:10.1002/chem.202103135.

## Intramolecular N–H...F Hydrogen Bonding Interaction in a Series of 4-Anilino-5-Fluoroquinazolines: Experimental and Theoretical Characterization of Electronic and Conformational Effects

Lorenz M. Urner<sup>[a]</sup>, Ga Young Lee<sup>[a]</sup>, Joseph W. Treacy<sup>[a]</sup>, Aneta Turlik<sup>[a]</sup>, Saeed I. Khan<sup>[a]</sup>, K. N. Houk<sup>[a]</sup>, Michael E. Jung<sup>[a]</sup>

<sup>[a]</sup>Department of Chemistry and Biochemistry, University of California, Los Angeles, CA 90095 (USA)

### Abstract

The 4-anilino-6,7-ethylenedioxy-5-fluoroquinazoline scaffold is presented as a novel model system for the characterization of the weak NH...F hydrogen bonding (HB) interaction. In this scaffold, the aniline NH proton is forced into close proximity with the nearby fluorine ( $d_{\text{H,F}} \sim 2.0 \text{ \AA}$ ,  $\angle \sim 138^\circ$ ), and a through-space interaction is observed by NMR spectroscopy with couplings ( $^1\text{h}J_{\text{NH,F}}$ ) of  $19 \pm 1 \text{ Hz}$ . A combination of experimental (NMR spectroscopy and X-ray crystallography) and theoretical methods (DFT calculations) were used for the characterization of this weak interaction. In particular, the effects of conformational rigidity and steric compression on coupling were investigated. This scaffold was used for the direct comparison of fluoride with methoxy as HB acceptors, and the susceptibility of the NH...F interaction to changes in electron distribution and resonance was probed by preparing a series of molecules with different electron-donating or -withdrawing groups in the positions *para* to the NH and F. The results support the idea that fluorine can act as a weak HB acceptor, and the HB strength can be modulated through additive and linear electronic substituent effects.

### Graphical Abstract

---

jung@chem.ucla.edu .

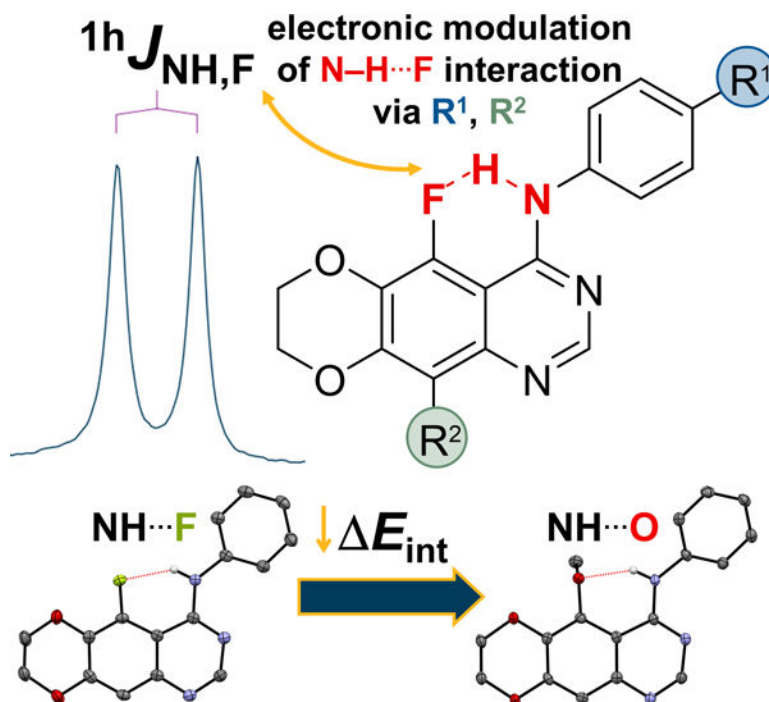
Supporting information for this article is available on the WWW under <https://doi.org/10.1002/chem.202103135>

This article belongs to a Joint Special Collection dedicated to François Diederich.

Dedicated to the memory of François Diederich.

Conflict of Interest

The authors declare no conflict of interest.



## Keywords

fluorine; hydrogen bonds; NMR spectroscopy; noncovalent interactions; quinazolines

## Introduction

Fluorine is becoming increasingly prevalent in the development of pharmaceuticals and agrochemicals; for example, 25 % of small-molecule drugs in the clinic contain fluorine.<sup>[1]</sup> Yet, the role of fluorine in one of the main noncovalent interactions (which is crucial for pharmacodynamic activity)-hydrogen bonding (HB)-has been a matter of much debate.

Although inorganic fluoride ion forms the strongest hydrogen bonds ( $45.8 \text{ kcal mol}^{-1}$ ),<sup>[2]</sup> covalently bound fluorine (organic fluorine) has only weak HB capability, if at all.<sup>[3]</sup> In fact, as stated by Dunitz, organic fluorine hardly ever forms HB interactions, as it is such a weak HB acceptor due to low basicity, low-lying lone pair orbitals, tightness of electron shell, and inability to modify by electron delocalization or polarization despite its very high intrinsic electronegativity.<sup>[4]</sup> However, analyses of X-ray crystal structures deposited in the Cambridge Structural Database (CSD), as well as theoretical and experimental studies (e. g., by NMR or IR spectroscopy), have shown that organic fluorine can form HB interactions with NH or OH donors, but only in the absence of any stronger competing HB acceptors.<sup>[5]</sup> On the other hand, in an analysis of protein-ligand interactions from the Protein Data Bank, no increased propensity of fluorine acting as a HB acceptor was found.<sup>[6]</sup>

Overall, the unambiguous identification and characterization of XH...F HB interactions (X=O, N) have led to controversial discussions, especially as these interactions could also be regarded as dipole-dipole or dispersive interactions.<sup>[5a,7]</sup> Recently, these anomalous

properties of organic fluorine were explained in terms of its very low polarizability and low charge capacity, which do not allow fluorine to become as negative (in partial charge) as anticipated.<sup>[8]</sup>

Nevertheless, NH...F interactions in bioactive compounds have been said to exert a profound influence not only on potency, but also on molecular properties such as permeability and conformation through a combination of electronic and steric effects, resulting in “shielding” of the NH proton.<sup>[9]</sup> Some examples from the literature which report on the influence of a fluorine on a nearby NH through a presumed intramolecular HB are depicted in Figure 1A, and comprise brain-penetrant EGFR kinase inhibitor **1** (increased CNS penetration),<sup>[10]</sup> IKK- $\beta$  inhibitor **2** (improved permeability),<sup>[11]</sup> and BACE-1 inhibitor **3** (improved permeability and efflux).<sup>[12]</sup>

Direct experimental observation of intramolecular NH...F interactions has been reported in carefully devised model systems with enforced, close intramolecular NH...F interactions that exclude the interference by stronger HB acceptors.<sup>[13]</sup> In these model systems, the close NH...F interaction has often been characterized by <sup>1</sup>H and <sup>19</sup>F NMR scalar couplings, which are denoted as <sup>1</sup>hJ<sub>NH,F</sub> to indicate that the spin-spin interaction is mediated by one hydrogen bond (1 h).<sup>[7,14]</sup> Some exemplary structures of different model systems are displayed in Figure 1B, and for each example the *J* coupling, the NH...F distance *d*, and N–H–F angle  $\alpha$  are indicated, as a means of comparing the strength or proximity of the interaction, and their geometrical parameters. Some of the findings from these and other related model systems that probe the NH...F interaction (in particular, by NMR, X-ray, or DFT methods) are that the *J* coupling is distance dependent (stronger for closer spatial proximity),<sup>[7]</sup> it is diminished in more polar solvents (as they can act as competitive HB acceptors),<sup>[15]</sup> and substituents can have an electronic influence on the strength of the HB interaction. However, the insights that have been extracted from these model systems for the intramolecular NH...F bond were often based on a specific set of typically a handful of compounds (the triad CH<sub>2</sub>F > CHF<sub>2</sub> > CF<sub>3</sub> is an example for substituents impacting the HB ability of fluorine),<sup>[16]</sup> and many of the analyzed interactions had an amide NH as HB donor. In these interactions, the carbonyl oxygen of the amide can be a competitive HB acceptor to fluorine as seen in solid-state structures, which then does not allow one to derive an unperturbed NH...F distance from crystal structure data. Therefore, it would be desirable to have additional model systems that provide further experimental and theoretical insights for the systematic characterization of this weak interaction.

Quite serendipitously, during one of our medicinal chemistry research programs on 4-anilinoquinazolines,<sup>[18]</sup> we noticed a remarkably strong through-space nuclear spin-spin coupling (<sup>1</sup>hJ<sub>NH,F</sub>) for a fluorinated anilinoquinazoline analogue. Based on this observation, we set out to prepare a series of related 4-anilino-6,7-ethylenedioxy-5-fluoroquinazolines, that we report in the present study for the characterization of the (aniline) NH...F interaction (Figure 1C). In particular, we aimed at investigating the energetic and geometrical characteristics of the NH...F interaction. We characterized the intramolecular NH...F hydrogen bond in apolar CDCl<sub>3</sub> and in polar [D<sub>6</sub>]DMSO solvents (as a competitive HB acceptor) by <sup>1</sup>H and <sup>19</sup>F NMR, in the solid state by X-ray crystal structure analysis for several of these analogues, and carried out DFT calculations to corroborate and extrapolate

our experimental results. Specifically, 1) we investigated the impact of conformation and steric congestion by comparison with reference compounds, 2) we probed the susceptibility of the NH...F interaction to changes in electron distribution and resonance by preparing a series of molecules with different electron-donating or -withdrawing groups in the *para* position of the aniline ring as well as the fused fluorobenzene moiety, and 3) we assessed the energy of the NH...F interaction computationally and also compared it with the NH...OMe interaction in a homologous analogue.

## Results and Discussion

### A difluorinated anilinoquinazoline analogue with intramolecular NH...F “through-hydrogen-bond” coupling that can be observed even in [D<sub>6</sub>]DMSO

During one of our recent medicinal chemistry programs on brain-penetrant EGFR tyrosine kinase inhibitors,<sup>[18]</sup> we tried to improve the metabolic stability of our lead compound **4** (JCN037) through introduction of a fluorine atom at position 5 of the quinazoline scaffold to obtain fluorinated analogue **5**. We were surprised to observe a pronounced downfield shift of the NH signal by 1.18 ppm in the <sup>1</sup>H NMR spectrum, and a strong splitting into a doublet with <sup>1</sup>*J*<sub>NH,F</sub> = 19.6 Hz (Figure 2 and Table 1). We suspected that the large coupling constant observed in compound **5** might have been a result of a through-space interaction, as it would be too large for a <sup>5</sup>*J*<sub>NH,F</sub> coupling mediated by the five covalent bonds between the fluorine and the NH proton.<sup>[17a,19]</sup> Similar large coupling constants have been described previously, such as in *ortho*-fluorobenzanilides with <sup>1</sup>*J*<sub>NH,F</sub> ~ 16 Hz (Figure 1B).<sup>[17a,20]</sup> Although the 2'-fluorine of **4** and **5** was not able to produce such a strong splitting as the 5-fluorine of compound **5**, closer inspection of the NH signal of **4** revealed a slightly-resolved doublet with <sup>1</sup>*J*<sub>NH,F(2')</sub> of 2.7 Hz, and the same coupling could be discerned in the NH signal of compound **5**, which therefore has to be described as a doublet of doublets with <sup>1</sup>*J*<sub>NH,F</sub> = 19.6, 2.6 Hz. Overall, the observed couplings of compound **5** correspond well with couplings observed in the structurally related fluorinated benzanilides.<sup>[17a,21]</sup> To further confirm the through-space contribution we performed decoupling experiments (<sup>1</sup>H {<sup>19</sup>F} and <sup>19</sup>F{<sup>1</sup>H} NMR) of compound **5**, which confirmed the NH...F interaction by the collapse of the NH signal into a broad singlet upon decoupling (Figure S1 in the Supporting Information). Although these decoupling experiments cannot distinguish between through-space or through-bond interaction, a <sup>1</sup>H, <sup>1</sup>H NOESY of compound **4** (Figure S2) confirmed the through-space interaction between NH and C(5)-H, and therefore the close proximity between these atoms. Based on these results, we then assumed that the NH and 5-fluoro of compound **5** are in a similar close proximity and can interact through-space. To further corroborate this hypothesis, we prepared a regioisomer of **5**, compound **S1** (Figure S3), in which the fluorine is attached at position 10 instead of position 5. Therefore, **S1** cannot form the same intramolecular NH...F interaction as in **5**, and in fact, the <sup>1</sup>H and <sup>19</sup>F NMR spectra of **S1** did not exhibit any <sup>6</sup>*J*<sub>NH,F</sub> coupling interaction (Figure S3). Although the F and NH of compound **S1** are separated by one more bond than in compound **5** (six vs. five bonds, respectively), we would still expect to see some residual coupling with the NH proton for **S1**, if it was a through-bond mediated <sup>5</sup>*J*<sub>NH,F</sub> interaction in **5**.

Another noteworthy observation in the  $^1\text{H}$  NMR spectrum of both **4** and **5** is the strongly downfield shifted C(6')-H on the aniline ring, which is indicative of an intramolecular hydrogen bond with N(3). Based on these observations (and additionally supported by the X-ray crystal structure shown in Figure 3), the NH and 2'-fluoro groups adopt a *syn*-periplanar orientation, which is probably a result of the combined interplay of the electrostatic repulsion between 2'-fluoro and N(3) and the weak intramolecular NH...F hydrogen bond interaction. This phenomenon is similar to amide NH...F interactions, where the carbonyl O can quite often restrict the conformation through electrostatic effects and reinforce the NH...F interaction, for example, in  $\alpha$ -fluoroamides<sup>[15,22]</sup> or -anilides.<sup>[9b,23]</sup> When  $[\text{D}_6]$ DMSO is used as NMR solvent, any intramolecular HB interactions should be lost due to competitive HB interactions with the highly polar solvent, and pronounced downfield shifts of NH protons should occur. This solvent-dependent chemical shift difference between  $\text{CDCl}_3$  and  $[\text{D}_6]$ DMSO is expressed by Abraham's parameter  $A_{\text{NMR}}$  to quantify the strength of intramolecular hydrogen bonds, and classifies them into strong ( $< 0.05$ ) or weak (0.05–0.15) intramolecular H-bonds.<sup>[24]</sup> In case of **4**, the NH was shifted by  $\delta = 2.26$  ppm (7.35 to 9.61 ppm), and coupling was not discernable anymore, yielding a sharp singlet (Figure 2 and Table 1). Conversely, the C(6')-H was shifted upfield, confirming the proposed C(6')-H...N(3) interaction observed in  $\text{CDCl}_3$ . On the contrary, the  $^1\text{H}$  NMR of compound **5** in  $[\text{D}_6]$ DMSO, revealed only a slight downfield shift of the N–H proton by  $\delta = 0.51$  ppm (8.53 to 9.04 ppm), and a still quite remarkably broad splitting was observable of  $^1\text{h}J_{\text{NH,F}} = 9.9$  Hz. With an  $A_{\text{NMR}}$  of 0.07, the NH proton does form weak hydrogen bonds in compound **5**.

The particularly strong shielding of the NH proton by the two fluorine atoms in compound **5** was discerned by X-ray crystal structure analysis (Figure 3). In comparison to the slightly longer NH...F distance in **4** (2.474 Å), the NH proton of **5** is sandwiched between the two fluorine atoms, resulting in short NH...F distances of 2.063 and 2.196 Å, respectively. Being completely shielded by the two fluorine atoms, the NH of **5** is prevented from participating in any other HB interactions, as opposed to compound **4**, where the NH is involved in a HB interaction with N2. Conversely, N2 of compound **5** is engaged in a halogen bonding interaction with Br (Br...N contact of 3.04 Å, and C–Br...N angle of 169°). Possibly, the availability of the NH proton for intermolecular HB interactions has implications on the packing and conformational orientation of the aniline ring. As shown in Figure 3, the aniline ring of **4** is skewed out of plane with a dihedral angle  $\theta = -31^\circ$ , whereas the aniline ring of **5** adopts an almost fully planar conformation with  $\theta = -6^\circ$ .

#### 4-Anilino-5-fluoroquinazolines as model compounds for the study of intramolecular NH...F hydrogen bonding interactions

Motivated by the observation of a close intramolecular NH...F interaction in compound **5** by both NMR and X-ray crystallography, we envisioned using this scaffold as a novel model system for the detailed and systematic study of aromatic fluorine-aniline NH hydrogen bond interactions.

As conformational restriction and steric compression can have a major impact on coupling strength (as shown in a more general context for cage-like compounds),<sup>[25]</sup> we wanted to

analyze the contribution of these effects on the NH...F coupling in our anilinoquinazoline compounds. Specifically, we were intrigued by the finding that compound **5** exhibited a stronger coupling with  $^1\text{H}J_{\text{NH,F}} = 19.6$  Hz than fluorinated benzanilides with  $^1\text{H}J_{\text{NH,F}} = 16$  Hz (Figure 1B). Therefore, we prepared structurally related dioxane-fused benzamides **6** and **7** as reference compounds (Table 2; synthesis described in the Supporting Information).

Furthermore, we prepared a series of analogues of compound **5** with different electron-donating or -withdrawing groups (EDG, EWG) *para* to the F and the NH for the systematic electronic modulation of the NH...F interaction (Scheme 1, compounds **8–22**). We hypothesized that a change in electron density of both the hydrogen bond donor and acceptor should have an impact on the energy of the hydrogen bond, which could be correlated to the measured magnitude of the  $J$  coupling constants in the  $^1\text{H}$  and  $^{19}\text{F}$  NMR spectra, respectively.<sup>[26]</sup> The sign of the coupling constant could be determined by specialized NMR correlation experiments (but which we have not performed in this study).<sup>[27]</sup>

Inspired by compounds **4** and **5**, we attached the ethylenedioxy group to all our model compounds. This substituted quinazoline scaffold would have an intrinsically increased electron density on fluorine, while the electron density on the NH group would be decreased compared to an unsubstituted non-heterocyclic (naphthalene) scaffold. Furthermore, some practical aspects of this scaffold are that it results in enhanced solubility, and facilitates more precise measurements of the  $J$  coupling constant by creating a simplified spin system, and facile preparation of analogues in substitution reactions.

The synthesis of the fluorinated anilinoquinazolines **8–22** is summarized in Scheme 1. Preparation of all other compounds mentioned in the manuscript is described in Section S2. Starting from commercially available 3-fluorocatechol, fluoroquinazolinone **23** was prepared in five steps (Scheme 1A; details reported in Scheme S1). Compounds **8–15** were made by chlorination of **23** with  $\text{POCl}_3$ , followed by substitution of chloroquinazoline **24** with different *para*-substituted anilines (Scheme 1B). Substituents at C(10), that is, in the *para*-position of the fused fluorobenzene ring, were introduced via two different routes (Scheme 1C). Bromination of quinazolinone **23**, followed by treatment with  $\text{POCl}_3$  gave **25**, which was substituted with aniline to yield the 10-bromo analogue **16**. The 10-cyano and 10-methyl analogues, **17** and **18**, were prepared by Pd-catalyzed cross-coupling of **16**. In a similar manner, quinazolinone **23** could also undergo a nitration-chlorination sequence to give **26**, and substitution with the aniline afforded the 10- $\text{NO}_2$  analogue **19**. Hydrogenation over Pd/C afforded the 10- $\text{NH}_2$  analogue **20**. In an effort to verify the additivity of the substituents on NH...F coupling, we prepared analogues **21** and **22**, with substituents at both the 4' - and 10-positions (Scheme 1D).

### Conformational restriction and steric compression result in shorter NH...F distances and stronger coupling

In order to assess the geometrical requirements of the NH...F interaction, and to analyze how much the large coupling constant of our fluorinated anilinoquinazolines was a result of enforced proximity, we compared the  $J$  coupling of quinazoline **11** with structurally

related reference compounds **6**, **7**, and **27–29** (Table 2; synthesis described in the Supporting Information). We compiled the  $J$  couplings and NH chemical shifts  $\delta$  (as a means of estimating the strength of the NH...F interaction) of these compounds in Table 2, together with the NH...F distance  $d$ , angle  $\alpha$ , and torsional angle  $\theta$ , that were obtained from X-ray crystal structures (except for compounds **28** and **29**, for which no crystal structures could be obtained; the position of the N–H proton was established with standard parameters). Some of these geometrical parameters might be different in solution. For example, in the structures of **6**, **7**, and **27**, a competitive HB with the carbonyl groups is observed in the X-ray crystal structures.

Unsubstituted benzamide **6** exhibited a coupling of  ${}^1\text{h}J_{\text{NHtrans,F}} = 8.0$  Hz ( $d = 2.25$  Å,  $\alpha = 119^\circ$ ), that was derived from the  ${}^{19}\text{F}$  NMR spectrum due to broad signals in the  ${}^1\text{H}$  NMR spectrum. The observed  $J$  coupling of **6** is comparable to couplings of related benzamides reported in the literature.<sup>[19,21]</sup> The relatively small coupling of **6** can be attributed to the low barrier of rotation around the amide bond and to exchange phenomena, which result in line broadening, and therefore diminish coupling. Benzanilide **7**, which has a *N*-phenyl substituent, is conformationally restricted to the (*Z*)-amide conformation, and accordingly coupling was almost doubled to  ${}^1\text{h}J_{\text{NH,F}} = 15.3$  Hz ( $d = 2.18$  Å,  $\alpha = 122^\circ$ ). Finally, further conformational restriction of **7** by removing the rotatable bond between the aryl and amide group ( $\theta = -31^\circ$ ) by cyclization onto the benzodioxane scaffold gave quinazoline **11** ( $\theta = 2^\circ$ ), which exhibited a large coupling  ${}^1\text{h}J_{\text{NH,F}} = 19.2$  Hz, and concomitantly a very short NH...F distance  $d = 2.01$  Å and larger angle  $\alpha = 138^\circ$ . These observations are in line with the criteria for hydrogen bonds, that is, the closer the X–H...Y angle is to  $180^\circ$ , the stronger the hydrogen bond and the shorter the H...Y distance.<sup>[28]</sup> These criteria were also corroborated by anilide **27**, for which no coupling was observed, probably due to the five-membered-ring system that results in a larger NH...F distance and smaller angle ( $d = 2.5$  Å,  $\alpha = 96^\circ$ ). The 4-aminoquinazoline **28** exhibited very broad signals, and no coupling information could be deduced. Although the acetylated derivative **29** should exhibit an increased NH acidity, and therefore a stronger HB interaction,<sup>[17c,29]</sup> we measured a smaller coupling value of  ${}^1\text{h}J_{\text{NH,F}} = 17.1$  Hz than that for **11**, which might be attributable to a nonplanar, twisted conformation of the amide group to relieve unfavorable steric interactions resulting in an elongation of the NH...F distance.<sup>[30]</sup> Taken together, the intramolecular NH...F interaction of our model compounds seem to fulfill the criteria defined for HB (distance, angle). However, the interaction is probably very weak, and only the high structural rigidity of the anilinoquinazoline core can force the NH and F into close proximity to form sufficiently strong interactions that can be easily observed by NMR. This distance dependency of the coupling is also evident from the plot of all our experimentally determined NH...F coupling and distance data (derived from X-ray crystal structures, Figure S4).

### Electron-donating or -withdrawing groups can modulate the NH...F interaction

Next, we wanted to investigate how tunable the NH...F interaction in our anilinoquinazoline system is towards the modulation of the electron density on the HB donor (NH) or acceptor (F) moieties. To this end, we prepared and characterized by  ${}^1\text{H}$  and  ${}^{19}\text{F}$  NMR (in  $\text{CDCl}_3$  and  $[\text{D}_6]\text{DMSO}$ ) a series of compounds with electron-donating ( $\sigma_p < 0$ ) or -withdrawing ( $\sigma_p > 0$ )



groups in the position *para* to the NH (compounds **8–15**, substituents R<sup>1</sup>, Table 3), or the F (compounds **11**, and **16–20**, substituents R<sup>2</sup>, Table 4), that were thought to exert an effect on the NH...F interaction strength through resonance, polarization, or inductive effects.

According to the NMR data summarized in Table 3, when *para* substituents R<sup>1</sup> on the aniline ring become more electron-withdrawing, the NH proton experiences an increased downfield shift and higher *J*-coupling in nonpolar CDCl<sub>3</sub>. This phenomenon can be rationalized by the fact that the NH proton becomes more acidic with increasing electron-withdrawing character of the 4' substituent and thus more strongly hydrogen bonding. On the other hand, the same trend is observed for the NH chemical shift in more polar and good hydrogen-bonding acceptor [D<sub>6</sub>]DMSO, but the *J* coupling follows an opposite trend, that is, <sup>1</sup>*J*<sub>NH,F</sub> is reduced from 12.4 Hz (R<sup>1</sup> = NMe<sub>2</sub>) to 6.0 Hz (R<sup>1</sup> = COMe), and is not detectable anymore for R<sup>1</sup> = NO<sub>2</sub>. It is likely that [D<sub>6</sub>]DMSO is a competing hydrogen bond acceptor as reflected in the reduction of *J* coupling as compared to that in CDCl<sub>3</sub>. The resulting competing HB interaction with [D<sub>6</sub>]DMSO becomes stronger with the better hydrogen bond acceptor O than F, resulting in a weakened NH...F interaction, in turn diminishing the *J* coupling with F. To model this would require an extensive study with explicit DMSO molecules, and we have not performed those computational studies. However, to further shed light on the influence of the solvent on *J* coupling in our fluorinated quinazoline series, we measured-as a representative example-a <sup>1</sup>H NMR of compound **10** in non-polar CCl<sub>4</sub> to exclude any solvent-dependent interaction on the coupling. With <sup>1</sup>*J*<sub>NH,F</sub> = 19.5 Hz (Table S1) the coupling is slightly larger than in CDCl<sub>3</sub> by ~ 0.6 Hz, and is in line with the expected trend of diminished coupling in more polar solvents. This result also corroborates the HB nature of the NH...F interaction.

Examining the NMR data in Table 4 (substituents R<sup>2</sup> at the 10-position) reveals that while the NH chemical shift, δ(NH), experiences a much more attenuated shift compared to the R<sup>1</sup> substituent analogues in Table 3, the *J* coupling follows a clear trend towards diminished coupling with increasing electron-withdrawing tendency of the R<sup>2</sup> substituent, in both CDCl<sub>3</sub> and [D<sub>6</sub>]DMSO. The change in electron density on fluorine can also be assessed by the <sup>19</sup>F NMR chemical shift, δ(F), and the relative change of δ(F) measured for the compounds in Table 4 is comparable to the data reported for *para*-substituted fluorobenzenes (δ(F) data is given in Tables S2 and S3). In that context, Dalvit and Vulpetti have found correlations between the <sup>19</sup>F NMR chemical shift and the propensity of more shielded fluorines to be observed in close contact to hydrogen bond donors in protein structures, whereas deshielded fluorines were predominantly found in close contact with hydrophobic side chains.<sup>[23,32]</sup> This so-called “rule of shielding” is also supported by our δ(F) and *J*-coupling data in Table 4, with more shielded fluorine exhibiting a stronger coupling and vice versa, for example, compound **20** versus **17**.

In an effort to see how additive the individual contributions of R<sup>1</sup> and R<sup>2</sup> on *J* coupling are, and with the ultimate goal to create an analogue with a very large coupling constant, we prepared two disubstituted compounds **21** (R<sup>1</sup> = COMe, R<sup>2</sup> = NO<sub>2</sub>), and **22** (R<sup>1</sup> = COMe, R<sup>2</sup> = NH<sub>2</sub>). The NMR data of these two compounds is reported together with the corresponding monosubstituted analogues, for better comparison, in Table 5. The additivity of the substituents for both δ(NH) and <sup>1</sup>*J*<sub>NH,F</sub> holds true for nonpolar CDCl<sub>3</sub>, and also for

$\delta(\text{NH})$  in polar  $[\text{D}_6]\text{DMSO}$ . However, the  $J$  coupling in the latter solvent does not seem to follow a linear additive effect for the substituents. With a  $J$  coupling of 21.2 Hz in  $\text{CDCl}_3$ , compound **22** exhibits the strongest  $\text{NH}\cdots\text{F}$  interaction of our series, as anticipated by the combined substitution with a strong electron acceptor for  $\text{R}^1$  and a strong electron donor for  $\text{R}^2$ .

To gain a more systematic understanding of the observed substituent effects, we employed DFT calculations as this method has been applied for similar NMR calculations in other recent studies.<sup>[15,17c]</sup> Our aim was to study a wider array of electron-withdrawing or donating  $\text{R}^1$  and  $\text{R}^2$  substituents in silico. We first optimized and calculated  $^1\text{h}J_{\text{NH,F}}$  for each of the 13 synthesized compounds listed in Tables 3 and 4 at the B3LYP/6-311 + +G(d,p) level of theory,<sup>[33]</sup> which has been previously employed for spin-spin coupling calculations.<sup>[34]</sup> The H-F spin-spin couplings were computed with the GIAO method.<sup>[34]</sup> The gas-phase computed  $J$  coupling values were in reasonable agreement with the experimental values measured in  $\text{CDCl}_3$ , with  $R^2 = 0.74$  (Figure 4A). Slight difference between the gas-phase calculated and the solution-phase experimental  $J$  coupling values might arise from the hydrogen bonding of the substituents with chloroform solvent. However, we would like to emphasize the typically poor performance of DFT for indirect spin-spin coupling calculations involving fluorine, and therefore improved computational methods might result in a better explanation of our experimental trends.<sup>[35]</sup>

We then extended the calculations to 17 functional groups ( $-0.83 \leq \sigma_p \leq 0.78$ ) on both the 4'- ( $\text{R}^1$  substituents) and the 10- position ( $\text{R}^2$  substituents) of the anilinoquinazoline system. The calculated  $^1\text{h}J_{\text{NH,F}}$  values were plotted against the Hammett constant  $\sigma_p$  (Figure 4B). We observed strong linear free energy relationships (LFER) for both  $\text{R}^1$  (blue) and  $\text{R}^2$  (green) substituents. Particularly,  $\text{R}^1$  substituents exhibit positive correlation with  $\sigma_p$ , as more electron-withdrawing substituents ( $\sigma_p > 0$ ) lower the electrostatic potential on the NH proton, and therefore, increase its HB donor ability. In contrast,  $\text{R}^2$  substituents show negative correlation with  $\sigma_p$ , as more electron-donating substituents ( $\sigma_p < 0$ ) enhance the negative electrostatic on F, and hence, increase its HB acceptor ability.<sup>[36]</sup> Notably, the modulation of  $^1\text{h}J_{\text{NH,F}}$  is more pronounced in the  $\text{R}^2$  substituents than in the  $\text{R}^1$  substituents according to our computational results, as indicated by a larger magnitude of the slope in Figure 4B ( $m = -1.8$  vs. 0.8, respectively). This is as expected, since the  $\text{R}^1$  substituents are more distant from the NH than the  $\text{R}^2$  substituents are from the F. Overall, the combined experimental and computational results suggest that: 1) the observed spin-spin coupling is due to the intramolecular  $\text{NH}\cdots\text{F}$  HB interaction, and 2) substituents *para* to both NH and F can modulate HB strength, and therefore  $^1\text{h}J_{\text{NH,F}}$  values by up to 3 Hz.

### Energetic nature of the $\text{NH}\cdots\text{F}$ interaction and comparison with $\text{NH}\cdots\text{OMe}$

Taking compound **11** as a model system, we calculated the intramolecular interaction energy ( $E_{\text{int}}$ ) at the B3LYP-D3/6-311 + +G(d,p) level of theory (Figure 5, and see the Supporting Information for computational details). It was found that, at the particular  $\text{NH}\cdots\text{F}$  geometry established in the rigid quinazoline structure, the HB interaction is repulsive with a calculated gas-phase  $E_{\text{int}}$  of  $+0.6 \text{ kcal mol}^{-1}$ ,  $\text{NH}\cdots\text{F}$  bond distance of 1.92 Å, and a bond angle of 136° (Figure 5A). In order to examine whether the  $\text{NH}\cdots\text{F}$  interaction could

be energetically favorable in a more flexible environment, we optimized and computed  $E_{\text{int}}$  for the intermolecular interaction in the truncated quinazoline (Figure 5B). Here, the HB interaction is attractive with a calculated gas-phase  $E_{\text{int}}$  of  $-4.3 \text{ kcal mol}^{-1}$ , with a longer distance (2.12 Å) and a bond angle of  $156^\circ$ .

Because we were curious how the energetics of the  $\text{NH}\cdots\text{F}$  interaction would compare with a strong HB acceptor such as O, we carried out the same calculations, as we did for **11**, for the homologous analogue **30**, having a methoxy group in place of the 5-fluoro group (Figure 5A' and B'). In both intramolecular and intermolecular cases, the  $\text{NH}\cdots\text{OMe}$  interaction is favorable with  $E_{\text{int}}$  of  $-1.4$  and  $-8.7 \text{ kcal mol}^{-1}$ , respectively, and therefore stronger than the  $\text{NH}\cdots\text{F}$  interaction. However, the small  $E_{\text{int}}$  of **30** is indicative that the intramolecular HB arrangement is geometrically non-ideal, and enforced by the rigid anilinoquinazoline scaffold.

In addition, we performed NBO analysis in order to determine the extent of the  $\text{n}_{\text{F}}-\sigma_{\text{NH}}^*$  interaction. For compound **11**, this contribution was  $4.7 \text{ kcal mol}^{-1}$  for the lone pair on F that has the greatest interaction with  $\sigma_{\text{NH}}^*$ . An analogous calculation was performed on compound **30**, and we found that the interaction energy of the lone pair that contributes the most to the  $\text{n}_{\text{O}}-\sigma_{\text{NH}}^*$  interaction was  $6.7 \text{ kcal mol}^{-1}$ . Taken together, these theoretical results support the idea that organic fluorine can form attractive HB interactions with NH as a donor, but geometrical parameters are critical. Also, these results confirm that organic fluorine is a weaker HB acceptor than oxygen.<sup>[5d]</sup>

During the attempt to prepare a 10-methoxy-5-fluoro-substituted quinazoline analogue, we isolated the 5-methoxy-substituted compound **30** (Scheme S4). An X-ray crystal structure of **30** was obtained, which allowed us to experimentally compare the HB ability of fluorine with oxygen (as a methoxy substituent) in the intramolecular  $\text{NH}\cdots\text{X}$  interaction both in solution as well as in the solid state. The relevant  $^1\text{H}$  NMR and X-ray-derived geometrical data for **11** (X=F), **30** (X=OMe), and the unsubstituted analogue **31** (X=H) as a reference, are summarized in Table 6. Whereas compound **31**, with no intramolecular HB interaction, has an  $A_{\text{NMR}}$  of 0.32, compound **11** has an  $A_{\text{NMR}}$  of 0.10, which classifies the  $\text{NH}\cdots\text{F}$  interaction as a weak intramolecular HB. Also, the geometrical parameters of **11** (distance, angle) are in line with the criteria for HB. However, in comparison to **11**, the NH of **30** is shifted more downfield in the  $^1\text{H}$  NMR ( $\text{CDCl}_3$ ) by  $\delta = 1.66 \text{ ppm}$  (8.22 to 9.88 ppm), and this results in an  $A_{\text{NMR}}$  of 0.02, which classifies the  $\text{NH}\cdots\text{OMe}$  interaction as a strong intramolecular HB. Nevertheless, the geometrical parameters of the  $\text{NH}\cdots\text{OMe}$  interaction of **30** are interestingly almost equal to the parameters of **11**. There is almost no difference in the reduction of the van der Waals (vdW) radius  $\left(\frac{d(\text{H}\cdots\text{X})}{r_{\text{H}} + r_{\text{X}}}\right)$  between **11** (0.78) and **30** (0.76). Therefore, the reduction of vdW radius alone does not necessarily correlate with how favorable these attractions are.

## Conclusion

In summary, we have reported an analysis of the intramolecular  $\text{NH}\cdots\text{F}$  interaction, both experimentally, by NMR spectroscopy and X-ray crystallography, and theoretically, by DFT

computations, by using a series of 4-anilino-5-fluoroquinazolines as a novel model system for this weak interaction. This scaffold forces the NH proton to point towards the fluorine atom, resulting in an overall unnaturally close interaction. Although this is an energetically unfavorable interaction, the large coupling of  $19 \pm 1$  Hz enabled us to study the tunability of the NH...F interaction systematically through electronic substituent effects. In particular, the series of R<sup>2</sup>-substituted compounds (*para* to fluorine) provided further experimental support for Dalvit and Vulpetti's "rule of shielding", as we found that increased electron density on fluorine (more shielded fluorine) correlated with stronger *J* coupling in these compounds.

However, the observed large *J* couplings in quinazoline derivatives are not solely due to the reinforced intramolecular HB interactions but also due to the propinquity of H and F. Although the NH...F interaction can be energetically favorable and tunable in nature, the intramolecular NH...F interactions in these particular quinazoline compounds are repulsive overall due to steric compression and the forced close proximity brought about by the overall conformational rigidity. This effect, nonetheless, causes the NH proton to be "shielded", as seen, for example, in the crystal structure of compound **5** (Figure 3B and B'), in which other competitive HB interactions can be prohibited, or by the coupling that is still present even in the polar solvent [D<sub>6</sub>]DMSO of up to 13 Hz. R<sup>1</sup> and R<sup>2</sup> substituents can enhance the relative contribution of the NH...F attraction compared to steric repulsion, and therefore can introduce more effective "shielding" of the NH proton. Further studies might be needed to rationalize the apparently greater effect of R<sup>2</sup> substituents on the NH...F interaction.

The experimental and theoretical comparison of F and OMe as HB acceptors in the NH...X interaction confirmed that O is a stronger HB acceptor than F. Importantly, our results support the idea that organic fluorine can be regarded as a weak HB acceptor. The large coupling constant, its distance dependence, directional preference (Table 2), and susceptibility to electronic effects correspond with the criteria for HB.<sup>[13,26]</sup>

We envision that the weak HB ability of F can be further exploited in pharmaceutical science or other areas, through the selective modulation of this interaction by suitable substituents, which might even be observable in some instances by NMR spectroscopy. The fine-tuning of this weak interaction could further enhance the biological activity, and physicochemical properties by using the "masking" effect of the NH proton for improved membrane permeability.

## Experimental Section

The synthesis and X-ray crystal structure data of compound **4** (JCN037) is reported in ref. [18]. The synthesis of compounds **5–31**, **S1**, and **S2** is described in the Supporting Information, which also provides characterization of the compounds, crystallographic data, NMR spectra, and computational details.

Deposition Numbers 2103282 (**5**), 2103283 (**6**), 2103286 (**7**), 2103281 (**8**), 2103287 (**11**), 2103284 (**27**), and 2103285 (**30**) contain the supplementary crystallographic data for this

paper. These data are provided free of charge by the joint Cambridge Crystallographic Data Centre and Fachinformationszentrum Karlsruhe Access Structures service.

## Supplementary Material

Refer to Web version on PubMed Central for supplementary material.

## Acknowledgements

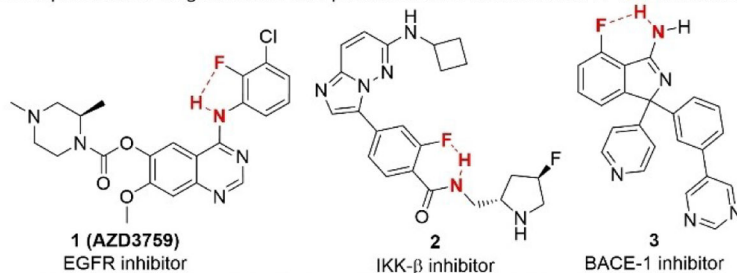
Dr. Yanpeng Xing is thanked for his helpful contributions with measuring NMR spectra. The authors also thank Frontier Scientific for the donation of boronic acid reagents. Calculations were performed on the Hoffman2 cluster at the University of California, Los Angeles. A.T. acknowledges the support of the National Institutes of Health under Ruth L. Kirschstein National Research Service Award F32GM134709.

## References

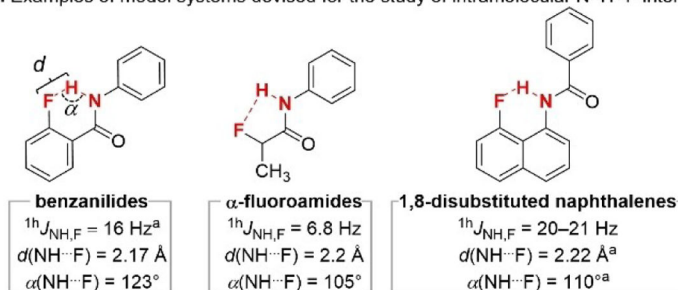
- [1]. Han J, Remete AM, Dobson LS, Kiss L, Izawa K, Moriwaki H, Soloshonok VA, O'Hagan D, J. Fluorine Chem 2020, 239, 109639.
- [2]. Dereka B, Yu Q, Lewis NHC, Carpenter WB, Bowman JM, Tokmakoff A, Science 2021, 371, 160–164. [PubMed: 33414217]
- [3]. Desiraju GR, Steiner T, IUCr Monographs on Crystallography, Vol. 9: The Weak Hydrogen Bond in Structural Chemistry and Biology, Oxford Science Publications, Oxford, 1999.
- [4]. a)Dunitz JD, Taylor R, Chem. Eur. J 1997, 3, 89–98;b)Dunitz JD, ChemBioChem 2004, 5, 614–621. [PubMed: 15122632]
- [5]. a)Schneider H-J, Chem. Sci 2012, 3, 1381–1394;b)Chopra D, Cryst. Growth Des 2012, 12, 541–546;c)Dalvit C, Vulpetti A, Chem. Eur. J 2016, 22, 7592–7601; [PubMed: 27112430] d)Taylor R, Acta Crystallogr. Sect. B 2017, 73, 474–488.
- [6]. Kuhn B, Gilberg E, Taylor R, Cole J, Korb O, J. Med. Chem 2019, 62, 10441–10455. [PubMed: 31730345]
- [7]. Hierso J-C, Chem. Rev 2014, 114, 4838–4867. [PubMed: 24533483]
- [8]. Murray JS, Seybold PG, Politzer P, J. Chem. Thermodyn 2021, 156, 106382.
- [9]. a)Müller K, Faeh C, Diederich F, Science 2007, 317, 1881–1886; [PubMed: 17901324] b)Böhm H-J, Banner D, Bendels S, Kansy M, Kuhn B, Müller K, Obst-Sander U, Stahl M, ChemBioChem 2004, 5, 637–643; [PubMed: 15122635] c)Gillis EP, Eastman KJ, Hill MD, Donnelly DJ, Meanwell NA, J. Med. Chem 2015, 58, 8315–8359; [PubMed: 26200936] d)Meanwell NA, J. Med. Chem 2018, 61, 5822–5880. [PubMed: 29400967]
- [10]. Zeng Q, Wang J, Cheng Z, Chen K, Johnström P, Varnäs K, Li DY, Yang ZF, Zhang X, J. Med. Chem 2015, 58, 8200–8215. [PubMed: 26313252]
- [11]. Shimizua H, Yamasakia T, Yonedaa Y, Muroa F, Hamadaa T, Yasukochib T, Tanakaa S, Tokia T, Yokoyamaa M, Morishitaa K, Iimura S, Bioorg. Med. Chem. Lett 2011, 21, 4550–4555. [PubMed: 21705219]
- [12]. Swahn B-M, Kolmodin K, Karlström S, von Berg S, Söderman P, Holenz J, Berg S, Lindström J, Sundström M, Turek D, Kihlström J, Slivo C, Andersson L, Pyring D, Rotticci D, Öhberg L, Kers A, Bogar K, von Kieseritzky F, Bergh M, Olsson L-L, Janson J, Eketjäll S, Georgievskaa B, Jeppsson F, Fälting J, J. Med. Chem 2012, 55, 9346–9361. [PubMed: 22924815]
- [13]. Champagne PA, Desroches J, Paquin J-F, Synthesis 2015, 47, 306–322.
- [14]. a)Dingley AJ, Cordier F, Grzesiek S, Concepts Magn. Reson 2001, 13, 103–127;b)Dra inský M, Annu. Rep. NMR Spectrosc 2017, 90, 1–40.
- [15]. Cosimi E, Trapp N, Ebert M-O, Wennemers H, Chem. Commun 2019, 55, 2253–2256.
- [16]. Dalvit C, Invernizzi C, Vulpetti A, Chem. Eur. J 2014, 20, 11058–11068. [PubMed: 25044441]
- [17]. a)Reddy GNM, Kumar MVV, Row TNG, Suryaprakash N, Phys. Chem. Chem. Phys 2010, 12, 13232–13237; [PubMed: 20820573] b)Chopra D, Row TNG, CrystEngComm 2008, 10, 54–67;c)Kazim M, Siegler MA, Lectka T, J. Org. Chem 2020, 85, 6195–6200. [PubMed: 32227992]

- [18]. Tsang JE, Urner LM, Kim G, Chow K, Baufeld L, Faull K, Cloughesy TF, Clark PM, Jung ME, Nathanson DA, ACS Med. Chem. Lett 2020, 11, 1799–1809. [PubMed: 33062157]
- [19]. Fritz H, Winkler T, Küng W, Helv. Chim. Acta 1975, 58, 1822–1824.
- [20]. Hennig L, Ayala-Leon K, Angulo-Cornejo J, Richter R, Beyer L, J. Fluorine Chem 2009, 130, 453–460.
- [21]. Mishra SK, Suryaprakash N, Molecules 2017, 22, 423.
- [22]. Banks JW, Batsanov AS, Howard JAK, O'Hagan D, Rzepa HS, Martin-Santamaria S, J. Chem. Soc. Perkin Trans 2 1999, 2409–2411.
- [23]. Dalvit C, Vulpetti A, ChemMedChem 2012, 7, 262–272. [PubMed: 22262517]
- [24]. Abraham MH, Abraham RJ, Acree WE Jr., Aliev AE, Leo AJ, Whaley WL, J. Org. Chem 2014, 79, 11075–11083. [PubMed: 25356529]
- [25]. Anet FAL, Bourn AJR, Carter P, Winstein S, J. Am. Chem. Soc 1965, 87, 5249–5250.
- [26]. Desiraju GR, Angew. Chem. Int. Ed 2011, 50, 52–59; Angew. Chem 2011, 123, 52–60.
- [27]. Kumari D, Hebbar S, Suryaprakash N, Chem. Phys. Lett 2012, 525–526, 129–133.
- [28]. Arunan E, Desiraju GR, Klein RA, Sadlej J, Scheiner S, Alkorta I, Clary DC, Crabtree RH, Dannenberg JJ, Hobza P, Kjaergaard HG, Legon AC, Mennucci B, Nesbitt DJ Pure Appl. Chem 2011, 83, 1637–1641.
- [29]. Herschlag D, Pinney MM, Biochemistry 2018, 57, 3338–3352. [PubMed: 29678112]
- [30]. Curran DP, Qi H, Geib SJ, DeMello NC, J. Am. Chem. Soc 1994, 116, 3131–3132.
- [31]. Hansch C, Leo A, Taft RW, Chem. Rev 1991, 91, 165–195.
- [32]. Dalvit C, Vulpetti A, ChemMedChem 2010, 6, 104–114.
- [33]. a)Becke AD, J. Chem. Phys 1993, 98, 5648–5652; b)Lee C, Yang W, Parr RG, Phys. Rev. B 1988, 37, 785–789.
- [34]. a)Sychrovský V, Gräfenstein J, Cremer D, J. Chem. Phys 2000, 113, 3530–3547; b)Helgaker T, Watson M, Handy NC, J. Chem. Phys 2000, 113, 9402–9409; c)Lantto P, Vaara J, Helgaker T, J. Chem. Phys 2002, 117, 5998–6009; d)Kupka T, Chem. Phys. Lett 2008, 461, 33–37; e)Kupka T, Magn. Reson. Chem 2009, 47, 674–683; [PubMed: 19431153] f)Nazarsky RB, Makulski W, Phys. Chem. Chem. Phys 2014, 16, 15699–15708. [PubMed: 24960547]
- [35]. a)Helgaker T, Jaszu ski M, Ruud K, Chem. Rev 1999, 99, 293–352; [PubMed: 11848983] b)Helgaker T, Jaszu ski M, Pecul M, Prog. Nucl. Magn. Reson. Spectrosc 2008, 53, 249–268; c)Vaara J, Phys. Chem. Chem. Phys 2007, 9, 5399–5418. [PubMed: 17925967]
- [36]. Wheeler SE, Houk KN, J. Chem. Theory Comput 2009, 5, 2301–2312. [PubMed: 20161573]
- [37]. Mantina M, Chamberlin AC, Valero R, Cramer CJ, Truhlar DG, J. Phys. Chem. A 2009, 113, 5806–5812. [PubMed: 19382751]

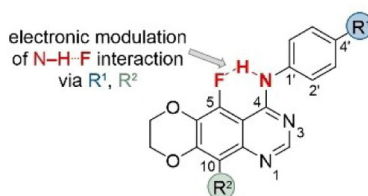
## A. Representative drug molecules with presumed close intramolecular N-H...F interactions



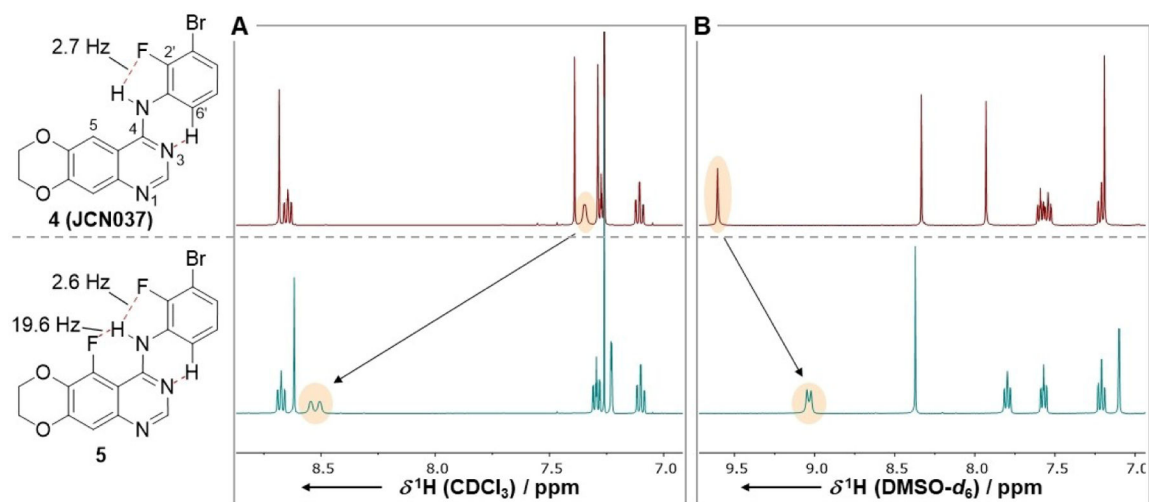
## B. Examples of model systems devised for the study of intramolecular N-H...F interactions



## C. Present study: series of 4-anilino-5-fluoroquinazolines with close N-H...F interactions

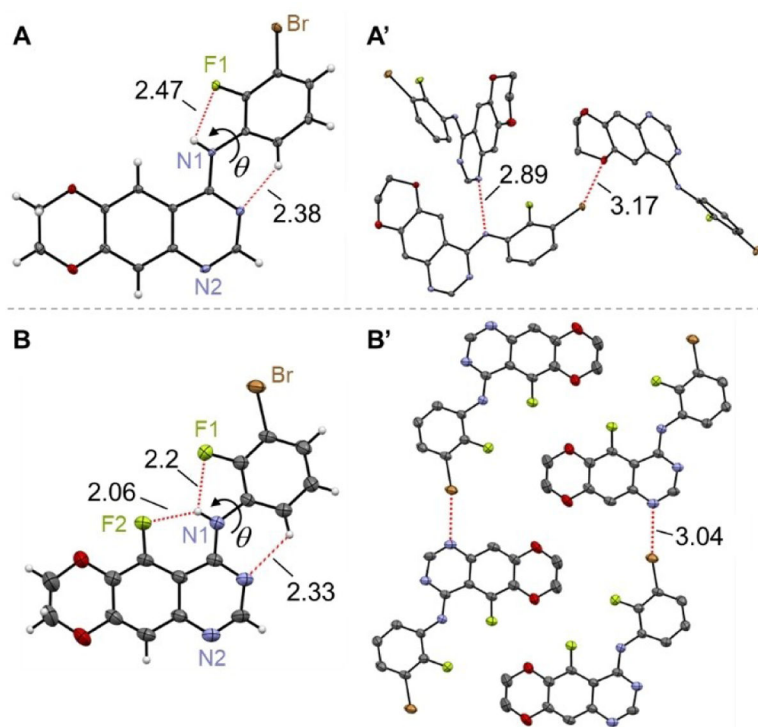
**Figure 1.**

Examples of compounds with intramolecular NH...F interactions. A) Drug molecules with reported increased membrane permeability due to shielding of the NH proton by fluorine. B) Selected examples of molecular model systems for the study of the intramolecular NH...F interaction.<sup>[15,17]</sup> Absolute coupling constants  $^1\text{h}J_{\text{NH},\text{F}}$ , and NH...F distance  $d$  and angle  $\alpha$  (from X-ray crystallographic data) are indicated for the depicted structure, or (a) a closely related analogue. C) NH...F interaction in 4-anilino-5-fluoroquinazolines presented in this study.  $\text{R}^1$ ,  $\text{R}^2$  are electron-donating/-withdrawing groups.

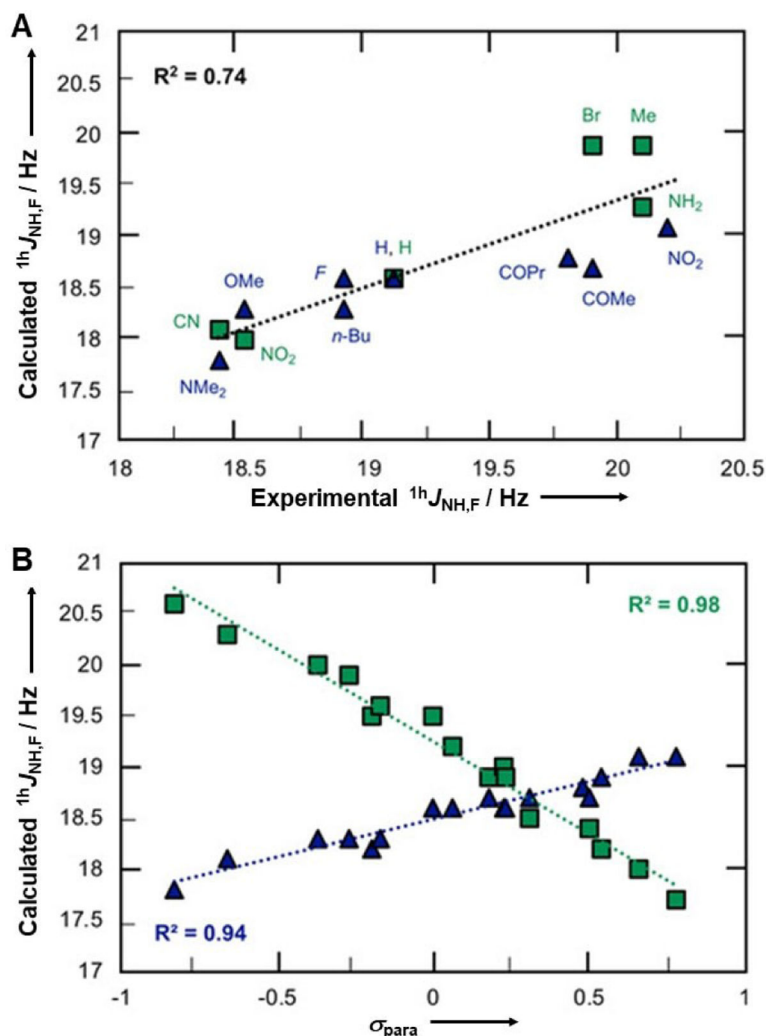


**Figure 2.** Splitting of the  $^1\text{H}$  NMR N–H signal by “through-hydrogen-bond” coupling with fluorine. A) Compound **4** shows a minor splitting of the NH signal in the  $^1\text{H}$  NMR in  $\text{CDCl}_3$ . Upon introduction of a fluorine at position 5 (compound **5**), the NH signal is shifted downfield, and a large splitting is observed. B) In  $[\text{D}_6]\text{DMSO}$ , no splitting was observed for compound **4**, whereas for compound **5**, the splitting was still present. Dashed red lines indicate close intramolecular interactions.

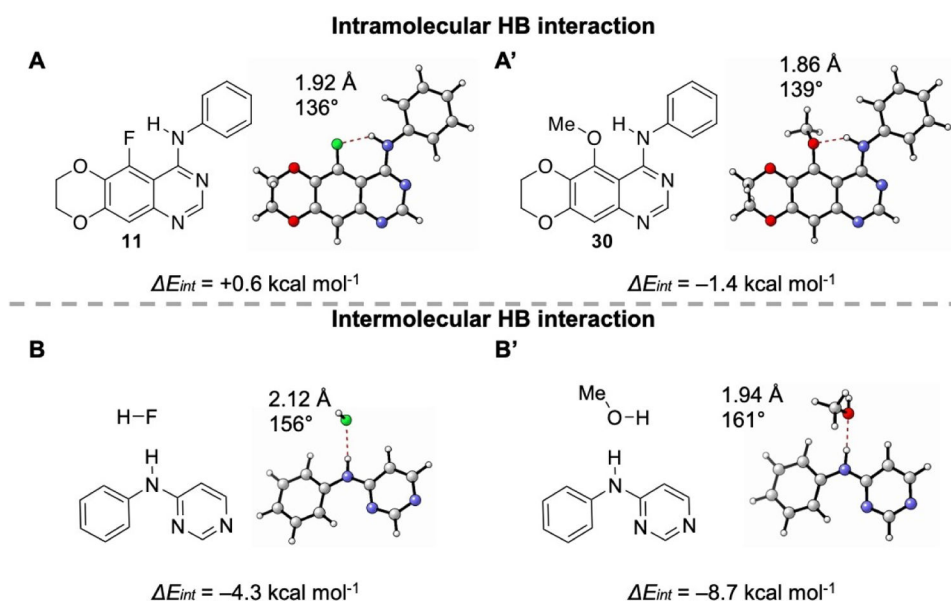




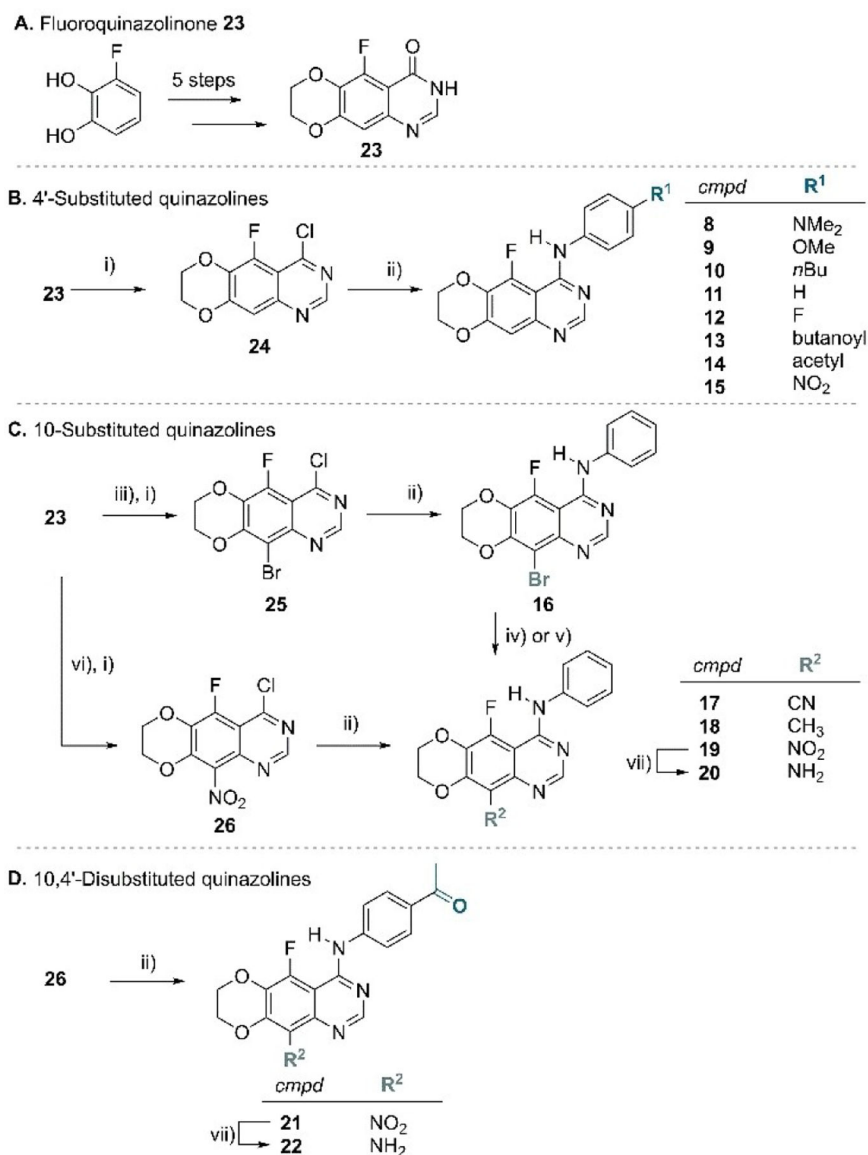
**Figure 3.** X-ray crystal structures of A) **4**, and B) **5**, with their packing arrangement shown in (A'), and (B'), respectively. 50 % probability ellipsoids; H atoms omitted for clarity in (A') and (B'). Selected distances [ $\text{\AA}$ ] are indicated by dashed lines. Selected angles [ $^\circ$ ]: A) N1–H...F1, 98(2); B) N1–H...F1, 114(3), N1–H...F2, 137(4).



**Figure 4.** Computed  $^1\text{H} J_{\text{NH,F}}$  values for 17 different substituents ranging  $-0.83 \leq \sigma_{\text{p}} \leq 0.78$  at both the 4'-(R<sup>1</sup>) and 10-position (R<sup>2</sup>) of the anilinoquinazolines. A) Correlation between gas-phase calculated and experimental (CDCl<sub>3</sub>) coupling constants  $^1\text{H} J_{\text{NH,F}}$ . B) LFER between gas-phase calculated  $^1\text{H} J_{\text{NH,F}}$  and  $\sigma_{\text{p}}$ . Quinazolines with different R<sup>1</sup> substituents (while R<sup>2</sup> = H) are shown as blue triangles. Quinazoline with different R<sup>2</sup> substituents (while R<sup>1</sup> = H) are shown as green squares. Geometry optimization and  $^1\text{H} J_{\text{NH,F}}$  calculations were performed at B3LYP/6-311++G(d,p) level.<sup>[33]</sup>



**Figure 5.** Computed energies of A), A') intra-, and B), B') intermolecular NH...F and NH...OMe interactions, respectively. Gas-phase geometry optimization and  $E_{int}$  calculations were performed with B3LYP-D3/6-311++G(d,p).

**Scheme 1.**

Synthesis of fluorinated quinazolines **8–22**, prepared from quinazolinone intermediate **23**. i) POCl<sub>3</sub>, DIPEA, toluene, 23 °C, 1 h, then 85 °C, 5 h, 73–99 %; ii) *para*-substituted aniline, HCl in dioxane, MeCN, 80 °C, MW, 30 min, 59–95 %; iii) NBS, DMF, 70 °C, 2.5 h, 89 %; iv) *t*BuXPhos-Pd-G3, *t*BuXPhos, K<sub>4</sub>[Fe(CN)<sub>6</sub>] · 3 H<sub>2</sub>O, KOAc, water, 1,4-dioxane, 100 °C, 3 h, 26 %; v) CH<sub>3</sub>BF<sub>3</sub>K, [PdCl<sub>2</sub>(dppf)] · CH<sub>2</sub>Cl<sub>2</sub>, Cs<sub>2</sub>CO<sub>3</sub>, water, THF, 80 °C, 44 h, 33 %; vi) 70 % HNO<sub>3</sub>, H<sub>2</sub>SO<sub>4</sub>, 23 °C, 11 h, 51 %; vii) Pd/C, H<sub>2</sub>, MeOH, EtOAc, 23 °C, 13 h, 30–88 %. DIPEA = *N,N*-diisopropylethylamine; dppf = - (diphenylphosphino)ferrocene; MW = microwave; NBS = *N*-bromosuccinimide.

**Table 1.**

Comparison of  $^1\text{H}$  NMR chemical shift and coupling constant, and derived Abraham's parameter, of  $\text{NH}\cdots\text{F}$  interaction observed in compounds **4** and **5**. n.d. not detected.

Cmpd	$\text{CDCl}_3$ $\delta_{\text{NH}}$ (ppm)	$^1J_{\text{NH,F}}$ [Hz]	$[\text{D}_6]\text{DMSO}$ $\delta_{\text{NH}}$ (ppm)	$^1J_{\text{NH,F}}$ [Hz]	$A_{\text{NMR}}$ (intraHB)
<b>4</b>	7.35	2.7	9.61	n.d.	0.31 (none)
<b>5</b>	8.53	19.6, 2.6	9.04	9.9	0.07 (weak)

**Table 2.**

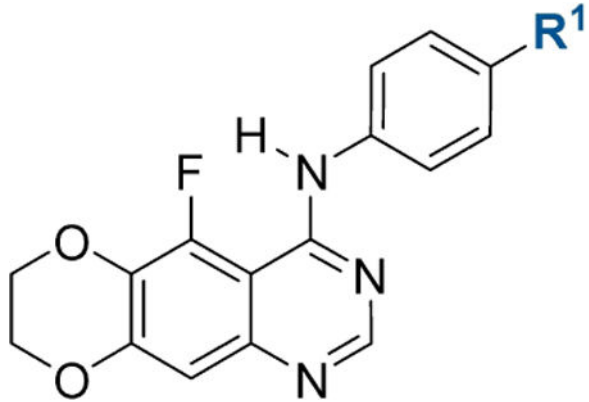
Comparison of NH...F interaction in benzamide **6**, benzanilide **7**, quinazoline **11**, and additional control compounds **27–29**. Data obtained from  $^1\text{H}$  and  $^{19}\text{F}$  NMR measurements ( $\text{CDCl}_3$ , 298 K), and X-ray crystal structure analysis (50 % probability ellipsoids; H atoms omitted for clarity except for NH; NH...F distance indicated by dashed line).

Cmpd	$\delta_{\text{NH}}$ (ppm)	$^1\text{h}J_{\text{NH,F}}$ [Hz]	$d_{\text{NH,F}}$ [ $\text{\AA}$ ]	$d_{\text{N,F}}$ [ $\text{\AA}$ ]	$\alpha_{\text{NH}\cdots\text{F}}$ [ $^\circ$ ]	$\theta$ [ $^\circ$ ]
<b>6</b>	6.56	8.0	2.25	2.77	119	32
<b>7</b>	8.31	15.3	2.18	2.76	122	-31
<b>11</b>	8.22	19.2	2.01 <sup>[a]</sup>	2.71 <sup>[a]</sup>	138 <sup>[a]</sup>	2 <sup>[a]</sup>
<b>27</b>	6.55	n.d.	2.5	2.73	96	-30
<b>28</b>	5.99	n.d.	n.a.	n.a.	n.a.	n.a.
<b>29</b>	8.85	17.1	n.a.	n.a.	n.a.	n.a.

<sup>[a]</sup> Averaged values from two independent structures. n.d. not detected; n.a. no data available.

**Table 3.**

Chemical shift and coupling data of 4'-substituted quinazolines.



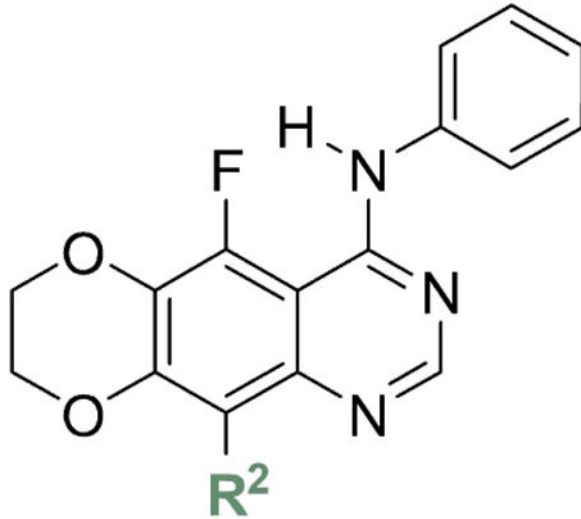
Cmpd	R <sup>1</sup>	$\sigma_p$ [31]	CDCl <sub>3</sub> $\delta_{NH}$ (ppm)	$^1J_{NH,F}$ [a] [Hz]	[D <sub>6</sub> ]DMSO $\delta_{NH}$ (ppm)	$^1J_{NH,F}$ [a] [Hz]
8	NMe <sub>2</sub>	-0.83	8.04	18.4	8.72	12.4
9	OMe	-0.27	8.07	18.5	8.83	11.9
10	<i>n</i> Bu	-0.16	8.16	18.9	8.86	12.0
11	H	0	8.22	19.1	8.93	11.7
12	F	0.06	8.13	18.9	8.97	11.0
13	COPr	0.48 [b]	8.41	19.8	9.21	6.6
14	COMe	0.50	8.43	19.9	9.22	6.0
15	NO <sub>2</sub>	0.78	8.54	20.2	9.50	n.d.

[a] Average from <sup>1</sup>H and <sup>19</sup>F NMR data.

[b] Hammett parameter of COEt. n.d. not detected.

**Table 4.**

Chemical shift and coupling data of 10-substituted quinazolines.



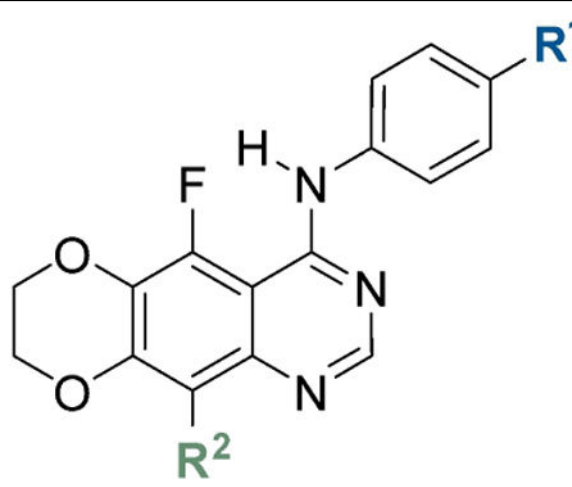
Cmpd	R <sup>2</sup>	$\sigma_p$ [31]	CDCl <sub>3</sub> $\delta_{NH}$ (ppm)	$^1hJ_{NH,F}$ [a] [Hz]	[D <sub>6</sub> ]DMSO $\delta_{NH}$ (ppm)	$^1hJ_{NH,F}$ [a] [Hz]
<b>20</b>	NH <sub>2</sub>	-0.66	8.42	20.1	8.78	13.4
<b>18</b>	Me	-0.17	8.26	20.1	8.90	12.5
<b>11</b>	H	0	8.22	19.1	8.93	11.7
<b>16</b>	Br	0.23	8.29	19.9	9.09	11.8
<b>17</b>	CN	0.66	8.20	18.4	9.22	10.1
<b>19</b>	NO <sub>2</sub>	0.78	8.22 <sup>[b]</sup>	18.5 <sup>[b]</sup>	9.25	10.5

<sup>[a]</sup> Average from <sup>1</sup>H and <sup>19</sup>F NMR data.<sup>[b]</sup> Data from crude sample mixture due to low solubility of purified sample.



**Table 5.**

Comparison of chemical shift and coupling data of 10,4'-disubstituted quinazolines **21** and **22** with corresponding monosubstituted analogues.



Cmpd	R <sup>1</sup>	R <sup>2</sup>	CDCl <sub>3</sub> δ <sub>NH</sub> (ppm)	<sup>1</sup> hJ <sub>NH,F</sub> [a] [Hz]	[D <sub>6</sub> ]DMSO δ <sub>NH</sub> (ppm)	<sup>1</sup> hJ <sub>NH,F</sub> [a] [Hz]
<b>11</b>	H	H	8.22	19.1	8.93	11.7
<b>14</b>	COMe	H	8.43	19.9	9.22	6.0
<b>19</b>	H	NO <sub>2</sub>	8.22 <sup>[b]</sup>	18.5 <sup>[b]</sup>	9.25	10.5
<b>20</b>	H	NH <sub>2</sub>	8.42	20.1	8.78	13.4
<b>21</b>	COMe	NO <sub>2</sub>	8.41 <sup>[b]</sup>	19.2 <sup>[b]</sup>	9.48	10.0
<b>22</b>	COMe	NH <sub>2</sub>	8.70 <sup>[b]</sup>	21.2 <sup>[b]</sup>	9.09	12.5

<sup>[a]</sup> Average from <sup>1</sup>H and <sup>19</sup>F NMR data.

<sup>[b]</sup> Data from crude sample mixture due to low solubility of purified sample in CDCl<sub>3</sub>.

Comparison of the fluoro and methoxy groups as intramolecular hydrogen bond acceptors. Data obtained from  $^1\text{H}$  NMR measurements ( $\text{CDCl}_3$ , 298 K), and X-ray crystal structure analysis. X-ray crystal structure of **30** drawn with 50 % probability ellipsoids;  $\text{NH}\cdots\text{O}$  distance indicated by dashed line.

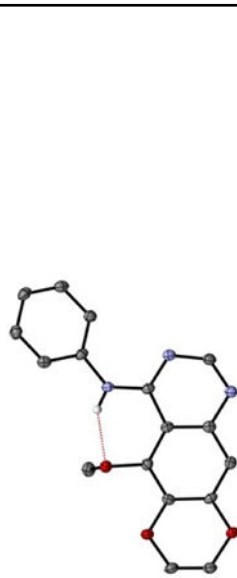
Table 6.

Compd	X	$\delta_{\text{NH}}$ (ppm)	$\text{CDCl}_3$	$[\text{D}_6]\text{DMSO}$	$A_{\text{NMR intramHB}}$	$d_{\text{H}\cdots\text{X}}$ [Å]	$d_{\text{N}\cdots\text{X}}$ [Å]	$\alpha(\text{N}\cdots\text{H}\cdots\text{X})$ [°]	$\alpha(\text{C}\cdots\text{X}\cdots\text{H})$ [°]	$d(\text{H}\cdots\text{X})/(r_{\text{H}}+r_{\text{X}})$ [a]
<b>11</b>	F	8.22		8.93	0.10 (weak)	2.01 [b]	2.71 [b]	138 [b]	98 [b]	0.78
<b>30</b>	OMe	9.88		9.97	0.02 (strong)	1.99	2.69	139	96	0.76
<b>31</b>	H	7.07 [c]		9.45	0.32 (none)	n.a.	n.a.	n.a.	n.a.	n.a.

[a]  $v_{\text{dW}}$  radii from ref. [37].

[b] Averaged values from two independent structures.

[c] Chemical shift of 4'-butyl-substituted analogue **S2** (reported in the Supporting Information) due to low solubility of **31** in  $\text{CDCl}_3$ .

X-ray crystal structure of **30**